

# Millimeter Wave Radar Combines Long Short-term Memory and Energy Storage Embedded System for On-street Parking Space Prediction

Yong-Ye Lin,<sup>1</sup> Min-Chi Wei,<sup>1</sup> Chi-Chia Sun,<sup>2\*</sup>  
Wen-Kai Kuo,<sup>3</sup> Fu-Chun Chan,<sup>4</sup> and Yen-Chih Liu<sup>5</sup>

<sup>1</sup>Graduate Institute of Electro-Optical and Material Science, National Formosa University  
No. 64, Wenhua Rd., Huwei Township, Yulin 632301, Taiwan

<sup>2</sup>Department of Electrical Engineering, National Formosa University  
No. 64, Wenhua Rd., Huwei Township, Yulin 632301, Taiwan

<sup>3</sup>Department of Electro-optical Engineering, National Formosa University  
No. 64, Wenhua Rd., Huwei Township, Yulin 632301, Taiwan

<sup>4</sup>Universität zu Lübeck Institut für Technische Informatik,  
Ratzeburger Allee 160, 23562 Lübeck, Germany

<sup>5</sup>Far Easy Pass Ltd., 2F., No. 99, Sec. 2, Sanmin Rd., Banqiao Dist., New Taipei City 22082, Taiwan

(Received September 6, 2021; accepted February 28, 2022)

**Keywords:** long short-term memory (LSTM), millimeter wave radar, portable photovoltaic energy storage, energy pool, programmable charging technology, autonomous cycle power supply

In this study, a millimeter wave radar was applied to detect the parking status and determine the availability of parking spaces. The data can be quickly uploaded to the cloud so that the parking status can be updated in real time. On the basis of cloud data, a long short-term memory (LSTM) model is built to perform deep learning. The LSTM can provide parking status prediction through the data and enable users to reserve parking spaces in advance, which can effectively increase the utilization rate of parking spaces by nearly 50%. The system can be quickly deployed, uses green energy, and is designed with a small portable photovoltaic (PV) energy storage system with programmable charging technology. To power the equipment, two long-term cycle battery packs are also included. When the remaining power of a battery pack is close to the minimum threshold, a programmable charging system activates the battery assembly and discharging mechanism while using the PV energy storage system to charge the unused battery pack. This design has the ability to extend the battery life by a factor of two, monitor the power status through the cloud, effectively alert technicians to replace batteries, and reduce maintenance labor requirements by 50%.

## 1. Introduction

We are attempting to find a way to allow customers to choose a parking location based on their preferences, park their vehicles quickly without having to search for an available parking space, and pay for their reservation of a parking space in advance to avoid queuing.

---

\*Corresponding author: e-mail: [ccsun@gs.nfu.edu.tw](mailto:ccsun@gs.nfu.edu.tw)  
<https://doi.org/10.18494/SAM3650>

We present a method of predicting real-time parking availability. This method consists of three subroutines for assigning simulated parking requests, estimating future departures, and predicting parking space availability. Parking requests are allocated iteratively using an aggregated approach as a function of simulated drivers' preferences and parking availability.

Martinetz *et al.*<sup>(1)</sup> used a machine learning approach to predict both the traffic status and the parking occupancy in Grand Lyon (France), whereas Yang *et al.*,<sup>(2)</sup> using long short-term memory (LSTM) and recurrent neural network (RNN) models to capture temporal features, were able to predict the street parking occupancy 30 min in advance. Inspired by the models used in Refs. 1 and 2, we adopt the LSTM model to predict an empty space and reduce the time spent by drivers on finding parking spaces.

Guan *et al.*<sup>(3)</sup> showed that a millimeter wave (mmWave) radar signal can have good propagation characteristics under low-visibility conditions, unlike common cameras and light detection and ranging (LiDAR) on the market; the latter cannot penetrate through dense fog. Referring to the approach of Guan *et al.*, we used a mmWave radar heat map to determine whether there is a car in a parking space. However, the system was mainly powered by batteries. We found that the power consumption of the mmWave radar is very high and the system batteries must be replaced frequently.

To avoid the complex process of system battery replacement, in this study, we propose an efficient portable energy storage system, which has advantages of simple assembly and disassembly, being wireless, and maintaining city aesthetics. This approach solves the problem of intermittent and unstable power and energy storage by continuously powering the equipment with renewable energy and providing power to the portable system. The most important component of the storage system is an energy pool that is like a reservoir that collects energy in any climate. When the system power is stable, the energy pool stores electrical energy. When the battery pack of the main system is depleted, the charged energy pool recharges the battery pack to keep the system power stable over time.

In Hong Kong, the Octopus card payment system has been integrated with the on-street parking payment system for many years, and it is considered to be one of the most successful smart on-street parking payment systems in the world. This research is dedicated to developing an even better system by combining a mmWave radar, an LSTM algorithm for a smart parking system, and a photovoltaic (PV) energy storage system to build a parking prediction system.

## 2. System Structure

In this section, we explain the reasons for using the mmWave radar and introduce the neural network and an in-depth understanding of LSTM operation. Heat maps are obtained through mmWave radar experiments to determine the presence of cars in parking spaces through numerical calculations and to provide real-time and future parking status predictions through different payment modes with LSTM. To solve the system problem, we propose a portable energy storage system to extend the life cycle of the power battery by using the charging technology of energy pool.

## 2.1 MmWave radar

The mmWave radar is a detection radar that operates in the millimeter wave frequency band. Usually, millimeter wave refers to the frequency domain of 30–300 GHz (wavelength of 1–10 mm).<sup>(4)</sup> This radar has some of the advantages of a microwave radar and an optical lightning sensor. The millimeter waveguide head is small and has light weight and high spatial resolution. In contrast to IR, laser, TV, and other optical guides, a millimeter waveguide has the ability to penetrate fog, smoke, and dust, and is suitable for all-weather conditions. In addition, its head interference and stealth resistance are also better than those of other microwave guides.

In this study, we use a TI-IWR6843AOPEVM<sup>(5)</sup> sensing module. The advantages of the mmWave radar are that it has a small antenna aperture, high tracking and guidance accuracy, easy low-elevation tracking, noise immunity, and high resolution for area identification and target monitoring. It also has a high information rate and an easy-to-use narrow pulse or broadband FM signal to obtain detailed structural characteristics of the target, a wide spectrum expansion capability, reduced multipath, enhanced noise interference resistance, easy to accurately monitor a target, and identification capability. The high Doppler frequency of the mmWave radar facilitates good detection and identification of slow and vibrating targets, and its ability to penetrate dry atmospheric pollution provides good detection capabilities in urban areas.

Zhang and Cao used micro-Doppler signatures obtained from the mmWave radar to detect the motion behavior of people,<sup>(6)</sup> and we adopt their approach, using the mmWave radar operating platform provided by TI, which is capable of converting micro-Doppler signatures into heat maps. The heat-map data have a much lower volume for data transmission and can be used for real-time application.

Even under dark conditions, the mmWave radar is better at detection than the other four sensors listed in Table 1. As shown by the table, the mmWave radar is not affected by weather or light conditions. It also has a detectable range of more than 100 m, the longest distance among the five sensors.

There are several methods of detecting the status of parking spaces. The best known is based on geomagnetism.<sup>(7)</sup> In this method, a wireless geomagnetic sensor is buried under the surface of a parking space and detects the arrival of a vehicle when it is parked from changes in magnetic field around the sensor, and sends a signal to a geomagnetic gateway installed at an appropriate location. Similarly, the geomagnetic sensor detects the departure of the vehicle from changes in magnetic field and notifies the geomagnetic gateway. The wireless geomagnetic sensor, a receiver, and the receiver base station form the data acquisition network, and the vehicle detector collects samples at a millisecond frequency to ensure the real-time status of parking spaces.

Table 2 shows a comparison of the performance characteristics of the mmWave radar and geomagnetic sensor. The cost of equipment is similar between these two sensors, but the maintenance cost of the geomagnetic sensor is higher than that of the mmWave radar. It takes a long time for workers to install a geomagnetic sensor in the ground, and when there is a problem with the sensor, it takes a whole day to dig it out for repair or replacement. The mmWave radar

Table 1  
Comparison of sensors.

Radar name	Infrared radar	Ultrasonic radar	mmWave radar	LiDAR	Camera
Cost	Low	Very Low	Medium	High	Medium
Detection angle	30°	120°	10–70°	15–360°	30°
Detection range	Close	Extremely close	Far	Far	Far
Night environment	High	High	High	High	Low
Road sign identification	X	X	X	X	V
Environmental limiting factors	Temperature	Wind, dust	Few limitations	Rainy day	Light
Advantages	Low cost, can be used normally at night	Cheap, simple structure, small size	Not affected by weather and night environment, detectable distance of more than 100 m	Accurate at long ranges, strong direction, fast response, not affected by ground noise	Moderate cost, can distinguish size and distance of obstacles and color
Disadvantages	Restricted by weather conditions, can only detect nearby objects, has difficulty in identifying pedestrians	Affected by weather and temperature changes, maximum measurement distance of only a few meters	Lower accuracy than LiDAR, reflected waves from pedestrians are weak and hard to detect	High cost, inoperable in fog, heavy snow, and rain	Similar to human vision, affected by visual field and weather factors

Table 2  
Comparison of detection methods.

	Equipment cost	Maintenance cost	Detection area	Accuracy	Data dimension	Life cycle cost
mmWave radar	Medium	Low	Large	High	Medium	Medium
Geomagnetic sensor	Low	High	Small	Medium	Medium	Medium

has a larger detection area than the geomagnetic sensor owing to its outstanding physical characteristics. Therefore, in this paper, the mmWave radar was chosen as the primary sensor to detect cars in on-street parking spaces.

## 2.2 LSTM recurrent network

Classical neural networks are based on the fact that data enters the network without any order, and the output depends only on the input features.<sup>(8)</sup> If the output depends on the features and previous outputs, classical feedforward neural networks are of no use. A possible solution to this problem is to use a neural network that can provide previous outputs recursively. Such a network, called an RNN,<sup>(9,10)</sup> was introduced by Hopfield in the 1980s and became popular in the early 1990s with improvements in back-propagation algorithms. Fig. 1 shows a schematic diagram of the concept of the LSTM.

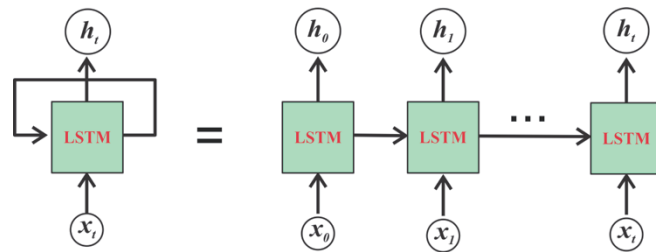


Fig. 1. (Color online) LSTM current network.

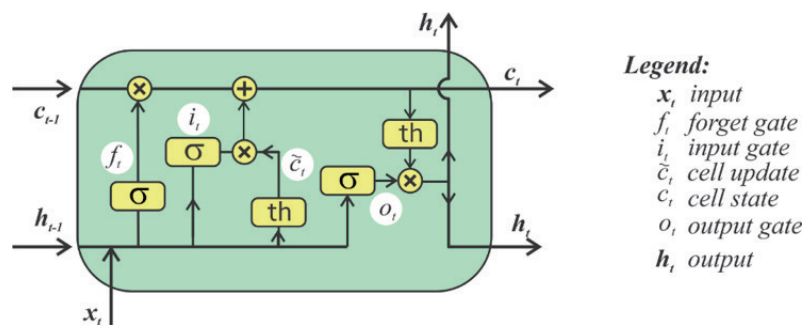


Fig. 2. (Color online) Legend of LSTM gate.

LSTM includes a common LSTM line, also known as the cell state, which is continuously updated with a nonlinear combination of its previous state and the current input and the hidden state of the module. These special units allow LSTM to ‘remember’ or ‘forget’ previous states, increasing its robustness in preserving useful data.<sup>(11)</sup> The current output of the RNN is defined by the current input  $x_t$  and also by states related to the previous network outputs  $h_{t-1}, h_{t-2}, \dots$

The RNN concept is simple and easy to implement, but problems arise during the training phase owing to unpredictable gradient behavior. During the training phase, the gradient problems of neural networks can be summarized into two categories: the vanishing and exploding gradient problems.

The RNN is based on the back-propagation algorithm, specially developed for the recurrent artificial neural network,<sup>(12)</sup> which is called back-propagation through time.<sup>(13)</sup> In the vanishing gradient problem, the parameter receives updates proportional to the gradient of the error, which in most cases is negligible, and results in the corresponding weights being constant, which stops the network from further training.

On the other hand, the exploding gradient problem refers to the opposite behavior, where the updates of weights (gradient of the cost function) take on larger values in each back-propagation step. This problem is caused by the explosion of the long-term components in the RNN.

The solution to the above problems is a specific design of their current network called LSTM.<sup>(14,15)</sup> One of the main advantages of LSTM is that it can provide a constant error flow. To provide a constant error flow, the LSTM cell contains a set of memory blocks with the ability to store the temporal state of the network. LSTM also has special multiplicative units called *gates* that control the information flow (Fig. 2).

An LSTM cell consists of the following five different formulas:

$$f_t = \sigma(W_f \cdot [h_{t-1}, x_t] + b_f), \quad (1)$$

the forget gate  $f_t$  sigmoid layer for time  $t$ , where  $f_t$  is calculated from the previous output  $h_{t-1}$ , the input vector  $x_t$ , and the matrix of weights from the forget layer  $W_f$  with the corresponding bias  $b_f$  added;

$$i_t = \sigma_g(W_i x_t + U_i h_{t-1} + b_i), \quad (2)$$

the input gate  $i_t$  sigmoid layer for time  $t$ , where  $i_t$  is calculated from the previous output  $h_{t-1}$ , the input vector  $x_t$ , and the matrix of weights from the input layer  $W_i$  with the corresponding bias  $b_i$  added;

$$o_t = \sigma_g(W_o x_t + U_o h_{t-1} + b_o), \quad (3)$$

the output gate  $o_t$  sigmoid layer for time  $t$ , where  $o_t$  is calculated from the previous output  $h_{t-1}$ , the input vector  $x_t$ , and the matrix of weights from the output layer  $W_o$  with the corresponding bias  $b_o$  added;

$$c_t = f_t \circ c_{t-1} + i_t \circ \sigma_c(W_c x_t + U_c h_{t-1} + b_c), \quad (4)$$

the cell state in time  $t$ , where  $c_t$  is calculated from the forget gate  $f_t$  and the previous cell state  $c_{t-1}$ . The results are summed as the input gate  $W_c$  and the cell update state, which is the tanh layer calculated from the previous output  $h_{t-1}$ , the input vector  $x_t$ , and the weight matrix for the cell with the addition of the corresponding bias  $b_c$ ;

$$h_t = o_t \circ \sigma_h(c_t). \quad (5)$$

The final stage of the LSTM cell is the calculation of the current output  $h_t$  by performing the multiplication operation  $\circ$  on the output gate layer, which is the tanh layer of the current cell state  $c_t$ . Since the looping of these five formulas is used in the parking space, it can be effectively used by citizens.

### 2.3 MmWave radar detection process

The mmWave radar detection process is shown in Fig. 3. When a parking space is empty, the system compares the UART protocol of the empty parking space with that of the mmWave radar to determine whether the parking space is empty or not, then sends the data to the background for recording.<sup>(16)</sup>

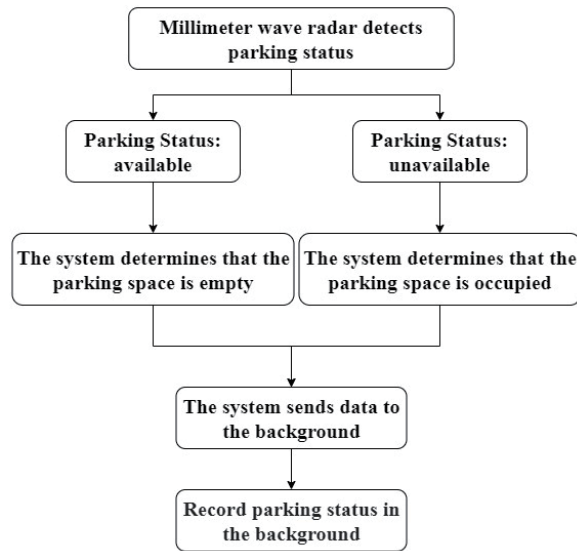




Fig. 3. Flow chart of mmWave radar detection.

Table 3  
(Color online) Radar detection UART protocol.

	Parking spaces are empty	Parking spaces are occupied
Test site		
UART Protocol	02 01 04 03 06 05 08 07 04 00 05 03 a0 06 00 00 43 68 0a 00 46 00 00 00 84 04 cb 53 1a 00 00 00 06 00 00 00 00 00 00 01 00 00 00 a0 01 00 00 00 00 00 00 c4 cd 84 3e 59 53 59 3d 00 00 00 00 63 25 1e 3c c6 a8 9c 3e 95 7f 28 3d 00 00 00 00 00 00 00 00 9c 84 b3 3e 38 bd 27 3d 00 00 00 00	02 01 04 03 06 05 08 07 04 00 05 03 e0 05 00 00 43 68 0a 00 77 00 00 00 f3 9c 35 8e 11 00 00 00 06 00 00 00 00 00 00 01 00 00 00 10 01 00 00 c2 8d 07 3c 1b bc 84 3e 76 61 59 3d 00 00 00 00 00 00 00 00 c0 1c 87 3f 65 1d e6 3e 00 00 00 00 00 00 00 00 c2 8a 3f d0 0a fd 3e 00 00 00 00

When a parking space is occupied, the system sends back the data in the mmWave radar protocol to determine if there is a car in the parking space, then sends the data to the backstage for recording.

The mmWave radar takes a measurement once per second, and each time, the radar UART protocol is compared with the previous data. When the information in the UART protocol is different from that in the previous measurement, as in Table 3, it determines whether the parking status has changed. When the parking status is found to have changed, the system changes the parking status and sends the new information to the backstage.



## 2.4 Portable energy storage system

To solve the power problem of the system, we propose the use of a solar-powered system. The sun's energy is abundant, free, clean, and renewable. Several manufacturers have upgraded their bollards by integrating solar power conversion systems.<sup>(17)</sup> The power systems of these machines are mainly completed by introducing solar PV panels. The most important factor is the efficiency of solar energy reception. This is because even a small shadow on a solar panel from neighboring buildings or natural features (such as trees) can almost completely stop electricity production. To improve the efficiency of solar energy reception, three solar panels were installed on the embedded system, one each on the top, left, and right sides, as shown in Fig. 4. As the sun moves throughout the day, the solar panels can effectively collect solar energy and charge the energy pool.

## 2.5 Energy pool

The emergence of energy storage systems, as shown in Fig. 5, has promoted the development of energy storage components, and energy storage technology not only compensates for the shortcomings of a single energy storage system that cannot meet the needs of many aspects of a power system, but also effectively extends the service life of energy storage devices. Therefore, the hybrid energy storage system (HESS), which has both high power density and high energy density, has become a hot spot of related research. Thus, we used an energy storage system composed of supercapacitors and lithium batteries as the main components of the energy storage system.<sup>(18)</sup>

An energy pool has functions of collecting, storing, and supplying electricity at the same time. It also has functions of collecting, storing, and taking electricity at the same time. In the case of long-term energy storage, the energy pool effectively extends the system power supply time. The super inner pool is a supercapacitor and the outer pool is a lithium battery. The purpose of using two batteries is to prevent the loss of energy overflow: solar energy is first charged into the outer battery; then, when the outer battery is fully charged, it is switched to the inner battery. The inner pool mainly supplies the EMS system and charges the battery pack in it.

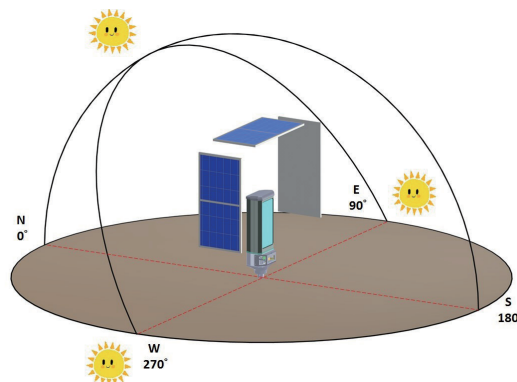


Fig. 4. (Color online) Solar azimuth angles for PV system.



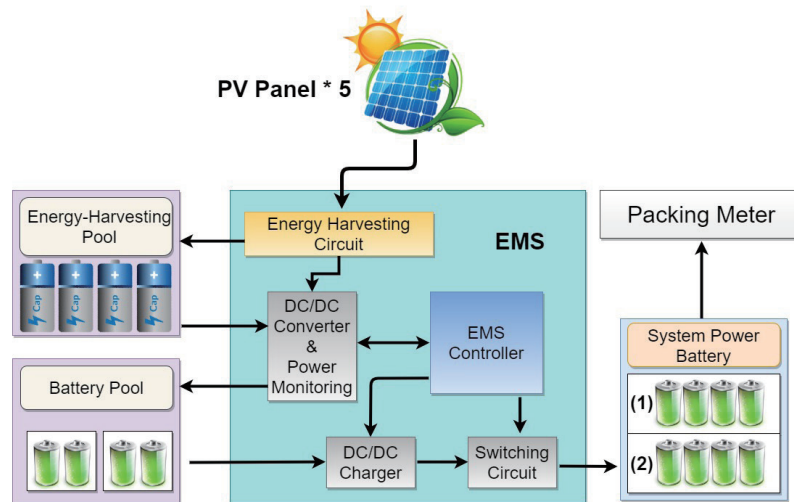


Fig. 5. (Color online) PV energy generation system.

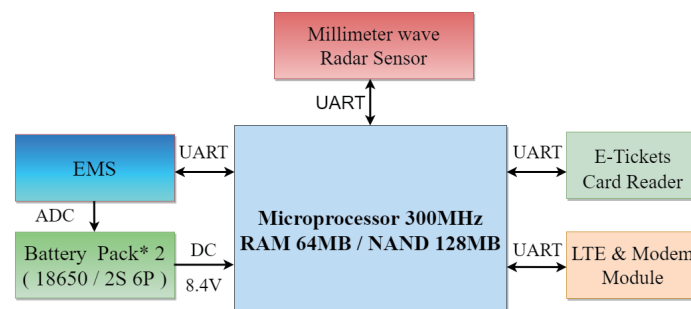


Fig. 6. (Color online) Embedded system.

The battery pack, which is the outer pool of the system, obtains energy from the inner pool to apply electricity to the embedded system for its normal operation.

## 2.6 Embedded system

As shown in Fig. 6, there are several modules in the low-power embedded system structure, including a display module, an LTE and modem module, an E-ticket and credit card reader, a camera and mmWave radar sensor, and two battery packs.

## 2.7 Payment

The prepayment of parking allows drivers to reserve a parking space so that they can avoid the difficulty in finding a parking space. In urban environments, drivers may spend a long time looking for parking spaces. According to our findings, most drivers who park in on-street parking spaces only need to park temporarily while they run errands, and they spend more time looking for parking spaces than they do dealing with their errands. With our system, drivers can

freely choose the location of the parking space by prepaying the parking fee, and they can also choose the temporary parking time to avoid the need to look for a parking space. Figure 7 shows the system payment flow. Figure 7(a) shows the general payment flow and Fig. 7(b) shows the prepayment flow, through the two different payment flows you can understand the parking status of users in this area.

Our smart parking system is located in a crowded food attraction area, where visitors usually stay for about 10–30 min. Owing to the high traffic flow during peak hours such as noon, visitors have to wait in line for a parking space for a longer period of time, causing traffic jams. By using the backend to check the parking space under normal circumstances, we found that the utilization rate was about 20 people on weekdays, but in the peak hours of 11:00 to 13:00, nearly 30 min of the parking space was not used, which was much larger than we expected. When parking spaces were available for reservation, the usage time was increased by almost half, effectively increasing the number of users.

### 3. Experimental Results

The experimental methods and data of the system are described in this section. In Sect. 3.1, we discuss the different mmWave radar heat maps obtained under different parking statuses. In Sect. 3.2, we predict the future parking status by analyzing the parking status record. In Sect. 3.3, we describe the portable energy storage system used to extend the system power usage time.

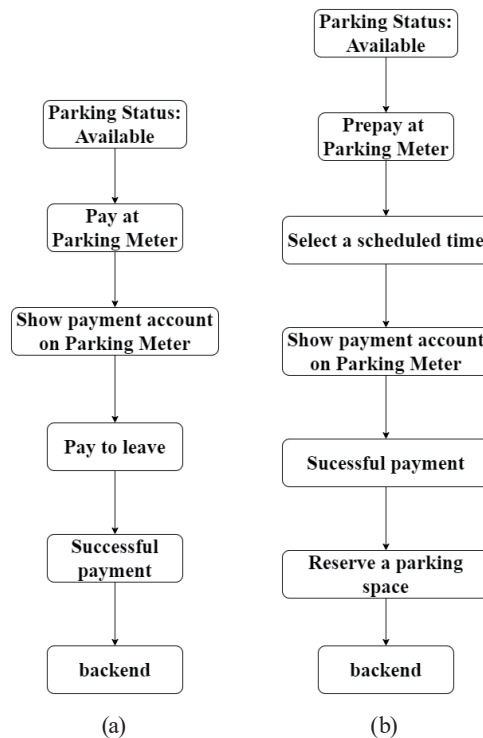


Fig. 7. Payment flow chart: (a) general payment procedure and (b) prepayment procedure.

### 3.1 MmWave radar experiment

In the use of the mmWave radar, there are several angles of detection that can be selected for reception and transmission to control the radar. Table 4 shows how different angles of the mmWave radar result in differences in reception and transmission. We choose the optimal transmit (Rx) and receive (Tx) angles of  $60^\circ$  and  $30^\circ$ , respectively, to detect cars in parking spaces.

As shown in Table 4, the radar's transmitting antenna has three of the four combinations; if the antenna is only open once, the effective measurement angle is  $60^\circ$  from the antenna vertically outward, and  $60^\circ$  up and down. If the antenna is open twice, two effective measurement angles ( $60^\circ$ ,  $30^\circ$ ) and ( $30^\circ$ ,  $60^\circ$ ) are obtained, resulting in the following two situations. Because the effective measurement area is located in the overlap of the two antenna measurement areas, if the effective measurement areas of the left and right antennas overlap, then the actual effective measurement angles are ( $60^\circ$ ,  $30^\circ$ ), and if the effective measurement areas of the upper and lower antennas overlap, then the actual effective measurement angles are ( $30^\circ$ ,  $60^\circ$ ). The second situation occurs when the antenna is fully open. Because the effective areas of the upper, lower, left, and right antennas overlap, the final actual measurement angles are ( $30^\circ$ ,  $30^\circ$ ).

For the first available space, the detection results of ( $30^\circ$ ,  $30^\circ$ ) and ( $30^\circ$ ,  $60^\circ$ ) are similar. Although the detection results of ( $60^\circ$ ,  $30^\circ$ ) and ( $60^\circ$ ,  $60^\circ$ ) are also similar, the strongest detection signal is found in the case of ( $30^\circ$ ,  $30^\circ$ ) owing to the reduction in the number of antennas from three to two. This results in lower energy recovery than in the case of three antennas. In the case of ( $60^\circ$ ,  $60^\circ$ ), there is only one antenna, resulting in the lowest signal recovery; in the case of ( $60^\circ$ ,  $60^\circ$ ), the signal recovery is lower than that in the case of ( $60^\circ$ ,  $60^\circ$ ).




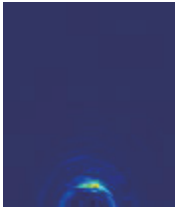


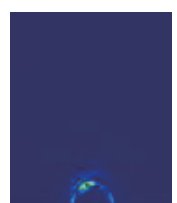




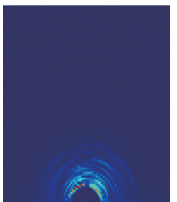
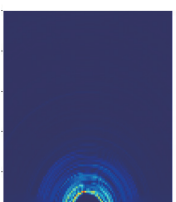



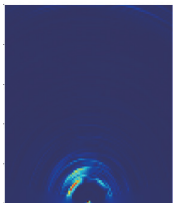

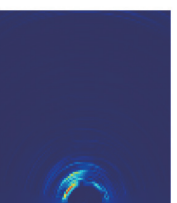
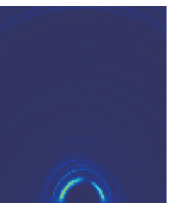

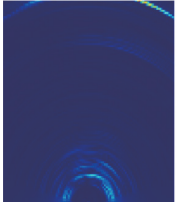

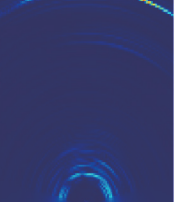

The different effective measurement angles are caused by the different numbers of antennas, and the same situation can be found in other locations (left side of the car, right side of the car, and both sides of the car).

Table 5 shows that the right side of the car is a special case in which there was interference from a sheet metal structure. The detection of the car position is clearly a smaller signal. Because there are more specific objects in front, it is more difficult to detect the car. From the above tests, it was found that there is a clear error in the detection of an empty parking space. Under normal circumstances, there should not be a strong signal from an empty space. We initially suspected that the metal material of the gutter cover caused the error. To verify this conjecture, the test was conducted at an empty position.

Table 4  
Radar parameters.

	Rx	Tx
4Rx3Tx	$30^\circ$	$30^\circ$
4Rx2Tx	$30^\circ$	$60^\circ$
4Rx2Tx	$60^\circ$	$30^\circ$
4Rx1Tx	$60^\circ$	$60^\circ$

Table 5  
MmWave radar detection results.

	4Rx3Tx (30°, 30°)	4Rx2Tx (60°, 30°)	4Rx2Tx (30°, 60°)	4Rx1Tx (60°, 60°)
 Both sides available				
 Left side occupied				
 Both sides occupied				
 Left side occupied				
 Right side occupied				

### 3.2 LSTM Experiment

From the LSTM prediction results, two weeks of parking results are used to produce data from real results, practice data, parking space reservations, and predicted data. The result shows the different times that cars park into the spaces.

If the parking status is created, then the parking space is not available. Conversely, if the parking status is ended, then the parking space is available (Fig. 8). Table 6 shows the status of the parking billing and closing data.

The parking space shown in Table 7 was reserved for 2 h. As shown in the first row of Table 7, the stop detection equipment will be billed on the basis of the pre-ordered time. When

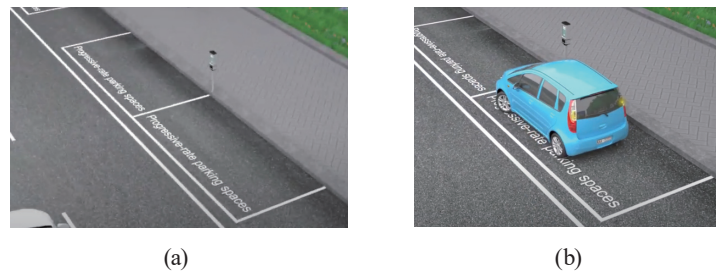


Fig. 8. (Color online) Parking status: (a) available and (b) unavailable.

Table 6  
Parking status data.

Year	Month	Day	Hour	Minute	Second	Position	Status
2021	05	01	08	03	06	stageInfo2	Create
2021	05	01	08	30	51	stageInfo2	End
2021	05	01	09	18	44	stageInfo2	Create
2021	05	01	09	46	24	stageInfo2	End
2021	05	01	09	49	56	stageInfo2	Create

Table 7  
Parking status of reservation data.

No	Year	Month	Day	Hour	Minute	Second	Reservation	Position	Status
1	2021	05	05	08	03	06	2 h	stageInfo2	Create
2	2021	05	05	10	03	06	Reservation time	stageInfo2	End
3	2021	05	05	09	50	44	Leave time	stageInfo2	End
4	2021	05	05	09	55	24	1 h	stageInfo2	Create
5	2021	05	05	10	55	24	Reservation time	stageInfo2	End

the status is created, the timer starts charging. As shown in the third row, the device automatically detects when a vehicle leaves a parking space early and then automatically flags the parking space as available. As shown in the fourth row, the parking space is then used by another vehicle. As shown in the fifth row, the pre-purchased parking time frame is 1 h.

These data can help us accurately predict the statuses of parking spaces at all times of the day as parking time pre-purchase is a short-term demand. There was little impact on the long-term predicted parking status (less than 1%).

To measure the parking flow, we set up the smart parking system in a tourist area on May 14, as shown in Fig. 9, indicating the extremum value to make the prediction data miss a little. As shown in Fig. 10, there was a steep decline on May 18. This sudden drop in parking space data was caused by the outbreak of COVID-19 in Taiwan because the pandemic led to a decrease in people's willingness to travel and a decrease in demand for tourism-related travel.

### 3.3 Portable energy storage system

Initially, all batteries in the system are fully charged. The PV system first charges the energy-harvesting pool. Figure 11 shows the solar panel installation location. After the battery pool has charged the system power battery, the battery pool can be charged with energy from the energy-

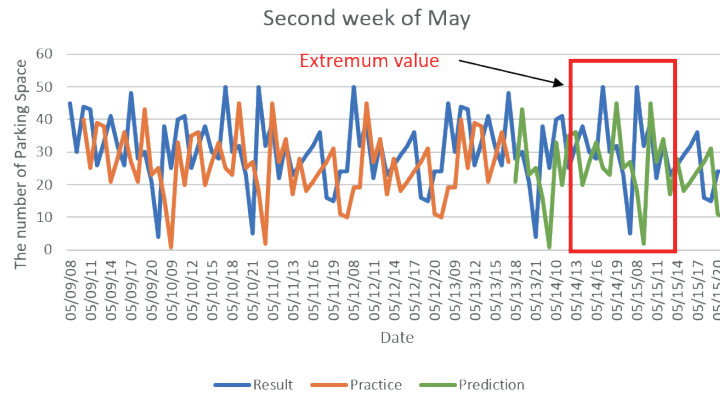


Fig. 9. (Color online) Second week of parking space data.

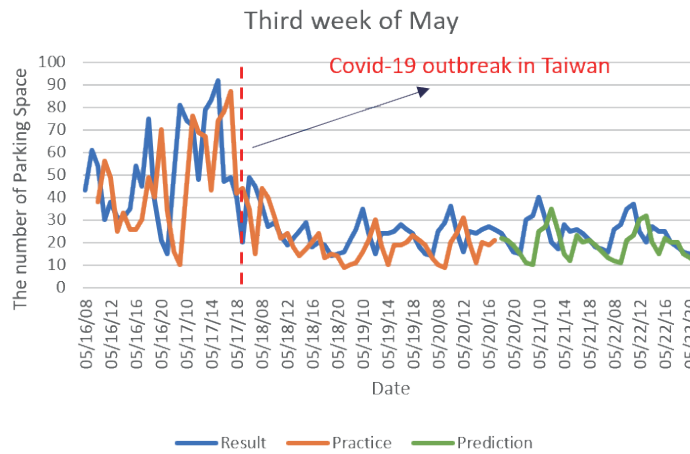


Fig. 10. (Color online) Third week of parking space data.

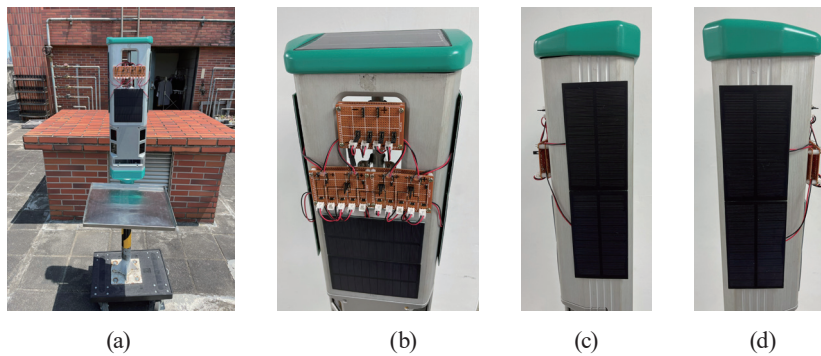


Fig. 11. (Color online) Solar panel installation location: (a) front side, (b) top side, (c) left side, and (d) right side.

harvesting pool. The whole test system is used to connect two series of six parallel battery packs with battery specifications of 7.4 V/33 Ah. The experimental results are in agreement with the design, with each group of energy pools designed to meet the battery pool group charging requirements with a supply of 1.5 times the energy. Under ideal conditions, the battery lifespan of the tested embedded system can be extended from 19 to 24 days, which greatly reduces the labor required to maintain the system as shown in Table 8 .



Table 8  
Comparison of energy uses in the embedded system.

Number of system battery pack format	Voltage	7.4	Ah	33	
States	Power W/h	Hours	Seconds	No. of transfers	Total power
1. Main PCB idle	0.19	24			4.56
2. Modem PCB transferring data	0.65	24	30	144	0.78
3. Main PCB changing the display	1.04		1	600	0.17
4. EPM performing transactions	5.39		60	60	5.39
5. Main PCB without modem, sensor PCB transferring data	0.28		600		0.05
6. Sending logs to OSDX and FTP servers	0.65		600		0.11
7. Credit card reader performing OTP	3.52		600		0.59
8. Camera taking photo	1.75		60	200	5.83
9. Radar scanning and data transfer	3.50	24	1	3600	3.50
Power consumption per day					20.98
Battery total power (two packs) only uses 80%					390.72
Before using EMS to expect service life per charge				18.62	Days
Charge for battery pack per day	11.84				W
Number of days X can be maintained after using EMS	42.76				Days

#### 4. Conclusion

We conducted several tests on on-street parking spaces. We found that the best way to detect cars is via the mmWave radar. This method shows very good detection results with high accuracy. For LSTM prediction results, in the future, our research team will investigate more effective methods to produce data that is more suitable for real-time situations, such as making the insertion time more detailed and changing the time resolution from hours to minutes or seconds. To solve the system power problem, we combined solar energy, batteries, and EMS-related technology, thus increasing the battery life of the system. In the future, we hope to apply this method to electronic products in various fields, so that electricity can be supplied continuously in places off the power grid, to improve the overall effect value and increase the utilization rate of PV power.

#### References

- 1 M. Martinetz, S. G-Berkovich, and K. Schulten: IEEE Trans. Neural Networks 4 (1993) 558. <https://doi.org/10.1109/72.238311>
- 2 S. Yang, W. Ma, X. Pi, and S. Qian: Transport. Res. Part C: Emerging Technol. 107 (2019) 248. <https://doi.org/10.1016/j.trc.2019.08.010>
- 3 J. Guan, S. Madani, S. Jog, S. Gupta, and H. Hassanieh: Proc. IEEE/CVF Conf. Computer Vision and Pattern Recognition (2020) 11464–11473.
- 4 R. Zhang and S. Cao: IEEE Access 7 (2019) 137065. <https://doi.org/10.1109/ACCESS.2019.2942382>
- 5 N. Yong, L. Yong, J. Depeng, S. Li, and V. Athanasios: Wireless Networks (2015) 2657. <https://doi.org/10.1007/s11276-015-0942-z>
- 6 C. Doer and F. Trommer: Radar Inertial Odometry with Online Calibration, 2020 European Navigation Conf. (IEEE, 2020) 110. <https://ieeexplore.ieee.org/document/9317343>
- 7 A. Sengupta, F. Jin, and S. Cao: A Dnn-LSTM Based Target Tracking Approach Using mmWave Radar and Camera Sensor Fusion (IEEE, 2019) 688–693.
- 8 F. Zhou and Q. Li: 2014 13th Int. Symp. Distributed Computing and Applications to Business (IEEE, 2014) 268–271.



- 9 S. Frank, L. Gang and Y. Dong: 12th Annu. Conf. International Speech Communication Association. (2011). <https://citeseerx.ist.psu.edu/viewdoc/download?doi=10.1.1.368.3047&rep=rep1&type=pdf>
- 10 C. Kyunghyun, B. Van Merriënboer, C. Gulcehre, D. Bahdanau, F. Bougares, H. Schwenk, and Y. Bengio: Learning Phrase Representations Using RNN Encoder-decoder for Statistical Machine Translation (aXiv, 2014). <https://arxiv.org/abs/1406.1078>
- 11 S. Alex: Fundamentals of Recurrent Neural Network (RNN) and Long Short-term Memory (LSTM) Network (Physica D: Nonlinear Phenomena, 2020) 132306.
- 12 S. Agatonovic-Kustrin, and R. Beresford: J. Pharm. Biomed. Anal. **22** (2000) 717. [https://doi.org/10.1016/S0731-7085\(99\)00272-1](https://doi.org/10.1016/S0731-7085(99)00272-1)
- 13 F. A. Gers, N. N. Schraudolph, and J. Schmidhuber: J. Mach. Learning Res. **3** (2002) 115. <https://www.jmlr.org/papers/volume3/gers02a/gers02a.pdf>
- 14 K. Greff, R. K-Srivastava, J. Koutník, B. R-Steunebrink, and J. Schmidhuber: A Search Space Odyssey (IEEE, 2017) 2222–2232. <https://ieeexplore.ieee.org/document/7508408>
- 15 Z. Huang, W. Xu, and K. Yu: Bidirectional LSTM-CRF Models for Sequence Tagging (aXiv, 2015). <https://arxiv.org/abs/1508.01991>
- 16 D. Frank: Serial and UART Tutorial (FreeBSD Documentation, 1996). <https://docs.freebsd.org/en/articles/serial-uart/>
- 17 C. A. Hill, M. C. Such, D. Chen, J. Gonzalez, and W. M. Grady: Battery Energy Storage for Enabling Integration of Distributed Solar Power Generation (IEEE, 2012) 850–857. <https://ieeexplore.ieee.org/document/6198748>
- 18 S. Koohi-Kamali, V. Tyagi, N. Rahim, N. Panwar, and H. Mokhlis: Renewable Sustainable Energy Rev. **25** (2013) 135–165. <https://www.sciencedirect.com/science/article/abs/pii/S1364032113002153>

## About the Authors



**Yong-ye Lin** received his M.S. degree in electrical engineering from St. John's University in 2010. He is currently pursuing his Ph.D. degree in the Graduate Institute of Electro-Optical and Material Science, National Formosa University. He is currently the director of R&D of Far Easy Pass Co., Ltd. His research interests are in payment system integration (public transportation, smart city, off-street parking, green energy technology, and Pedelecs). ([ecb1359@gmail.com](mailto:ecb1359@gmail.com))



**Min-chi Wei** received his M.S. degree in electrical engineering from National Formosa University in 2009. He is currently pursuing his Ph.D. degree in the Graduate Institute of Electro-Optical and Material Science, National Formosa University. His research interests are in the application of photoelectric sensing and the discussion of fire prevention strategies and applications in open spaces. ([wei0953074888@gmail.com](mailto:wei0953074888@gmail.com))



**Chi-chia Sun** received his B.S. and M.S. degrees in computer science and engineering from National Taiwan Ocean University in 2003 and 2004, respectively, and in electronic engineering from National Taiwan University of Science and Technology in 2006. From 2008 to 2011, he worked as a research assistant at Dortmund University of Technology and received his Doktor Ingenieur degree with DAAD full scholarship. He is currently a professor in electrical engineering at National Formosa University. His research interests are in FPGA system integration, Internet of Things, robotics, image processing, and FPGA/MCU PCB design. ([ccsun@gs.nfu.edu.tw](mailto:ccsun@gs.nfu.edu.tw))



**Wen-Kai Kuo** received his Ph.D. degree in electronics engineering from National Chiao Tung University in 1999. He is currently a professor in electro-optical engineering at National Formosa University. His research interests are in electro-optic probing techniques, photoelectric sensors, high-frequency mixed-mode IC design, and micro-opto-electro-mechanical systems. ([wkkuo@nfu.edu.tw](mailto:wkkuo@nfu.edu.tw))



**Fu-Chun Chan** received his B.S. and M.S. degrees in electrical engineering from National Formosa University (2014–2020). He is currently pursuing his Ph.D. degree in Universität zu Lübeck with full Doktor scholarship. His research interests are in computer science, Internet of Things, robotic image processing, and plant electrophysiology. ([erik748596@gmail.com](mailto:erik748596@gmail.com))



**Yen-Chih Liu** received his B.S. degree in electrical engineering from National Formosa University in 2021. He also worked as an intern at Far Easy Pass Co., Ltd. (2019–2020), where he is currently a firmware assistant engineer. His research interests are in computer science, Internet of Things, robotics, and embedded systems. ([40625149@gm.nfu.edu.tw](mailto:40625149@gm.nfu.edu.tw))